Design of Pyrazine Cocrystals of Enzalutamide –a lead from 1, 4-dioxane Solvates

Jupally Prashanth [ab], Alexander P. Voronin [c], Artem O. Surov [c*], Sridhar Balasubramanian [ab*]

[a]Centre for X-ray Crystallography, Department of Analytical & Structural Chemistry, CSIR-Indian Institute of Chemical Technology, Tarnaka, Uppal Road, Hyderabad-500007, Telangana, India.

[b]Academy of Scientific and Innovative Research (AcSIR) Ghaziabad 201002 (India)

[c]G.A. Krestov Institute of Solution Chemistry RAS, 153045, Ivanovo, Russia.
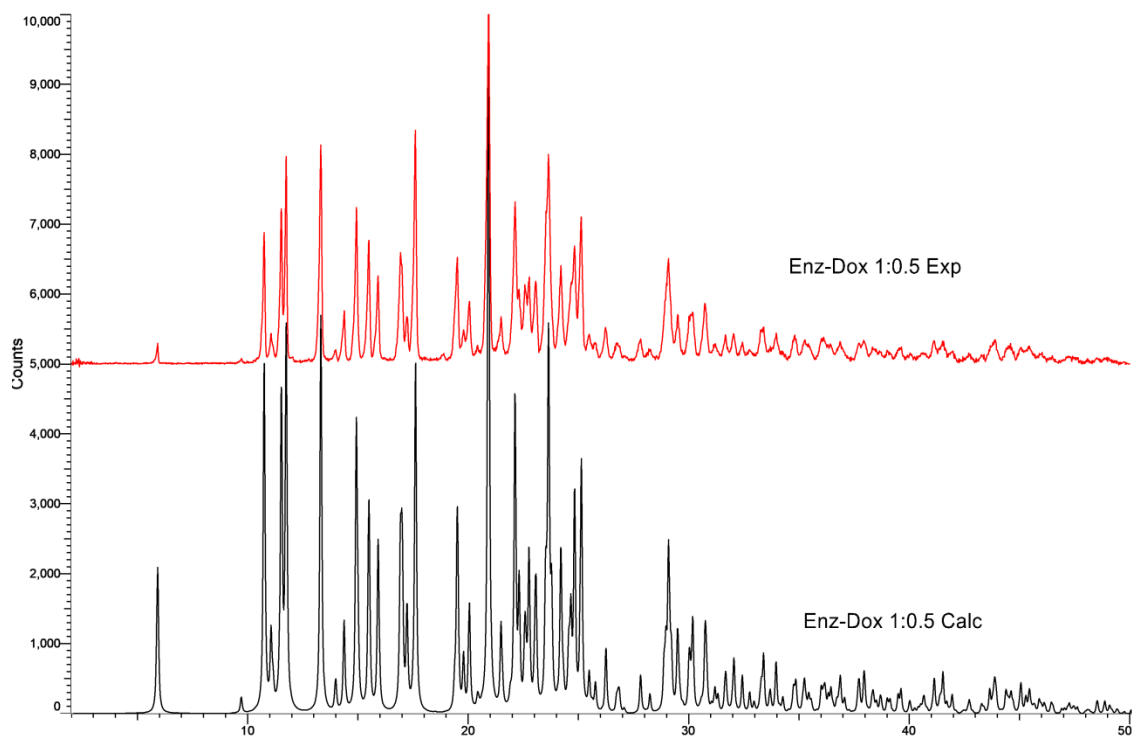
Figure S1. PXRD overlay of Enz-Dox 1:0.5 simulated pattern (Enz-Dox 1:0.5 Calc) with the phase pure experimental pattern (Enz-Dox 1:0.5 Exp).
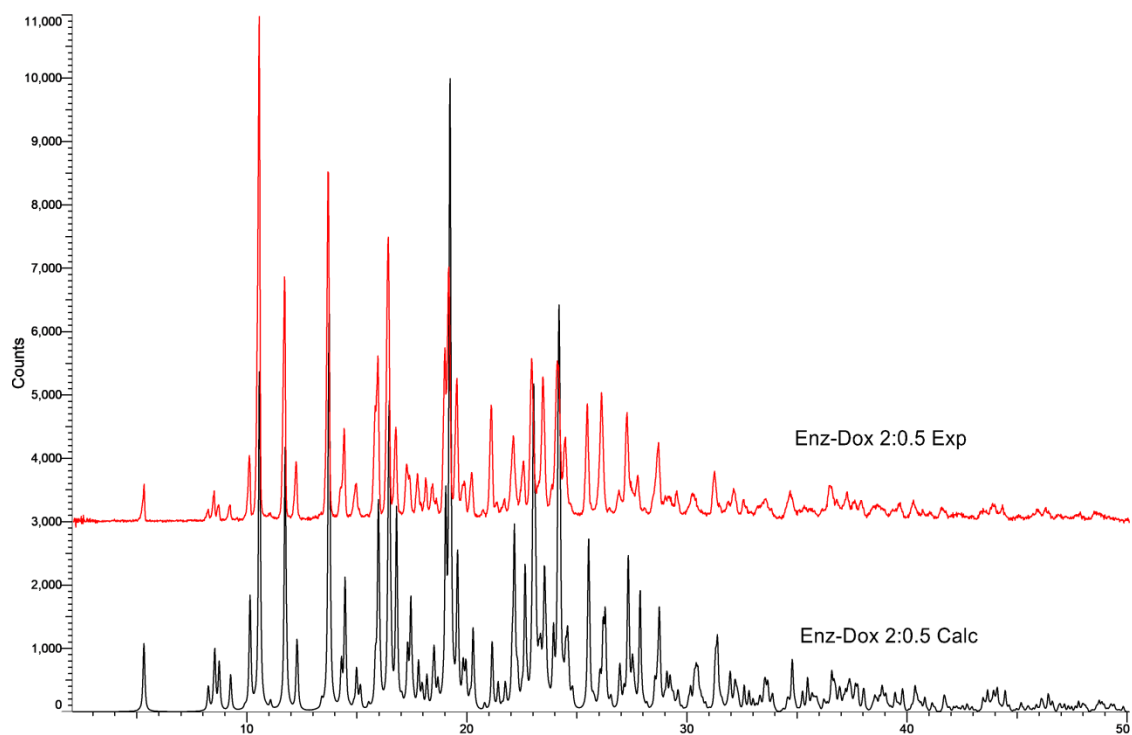

Figure S2. PXRD overlay of Enz-Dox 2:0.5 simulated pattern (Enz-Dox 2:0.5 Calc) with the phase pure experimental pattern (Enz-Dox 2:0.5 Exp).
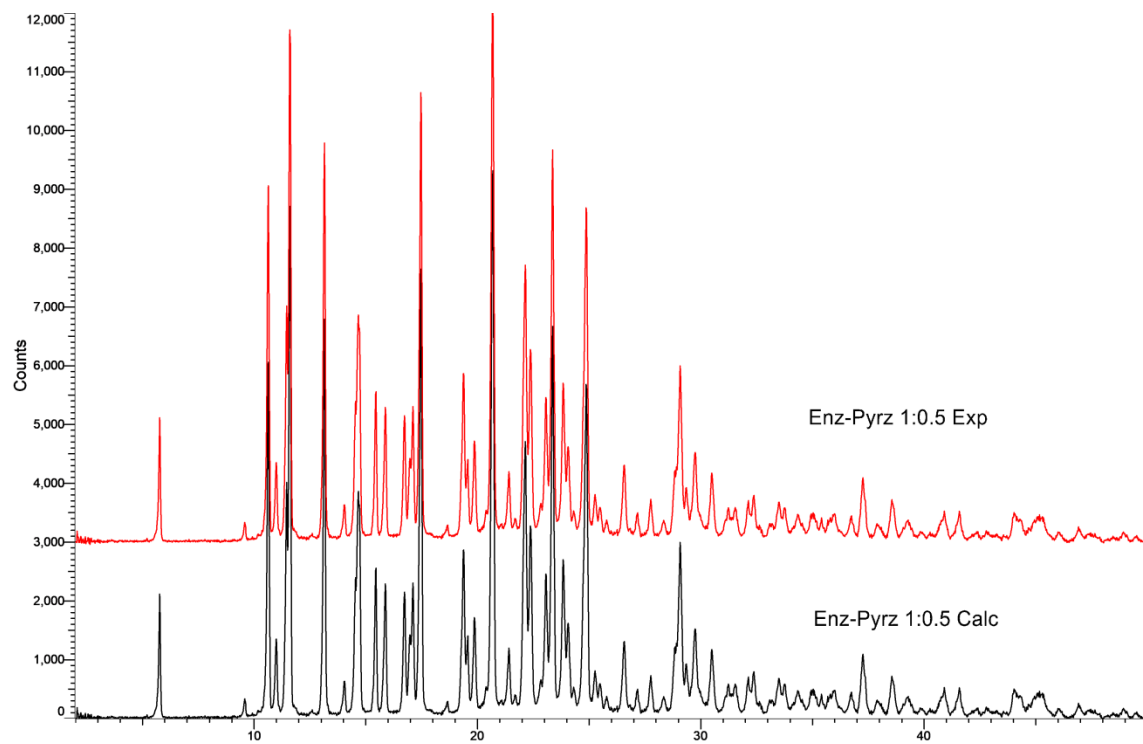
Figure S3. PXRD overlay of Enz-Pyrz 1:0.5 simulated pattern (Enz-Pyrz 1:0.5 Calc) with the phase pure experimental pattern (Enz-Pyrz 1:0.5 Exp).
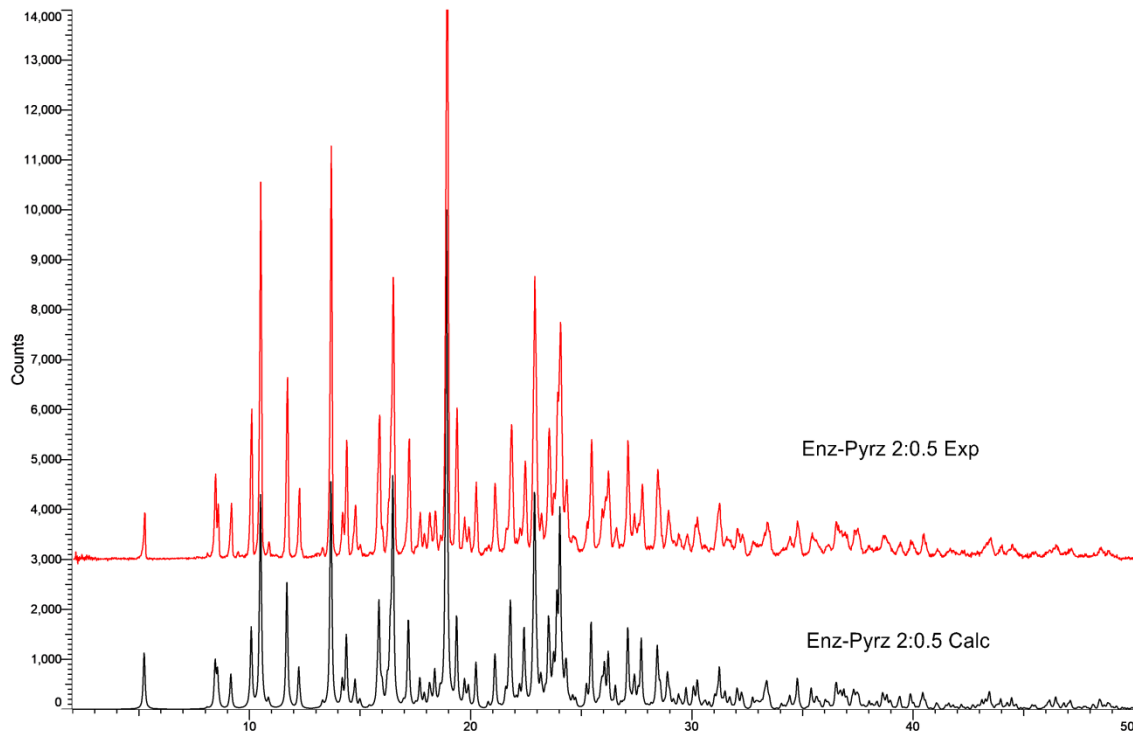

Figure S4. PXRD overlay of Enz-Pyrz 2:0.5 simulated pattern (Enz-Pyrz 2:0.5 Calc) with the phase pure experimental pattern (Enz-Pyrz 2:0.5 Exp).
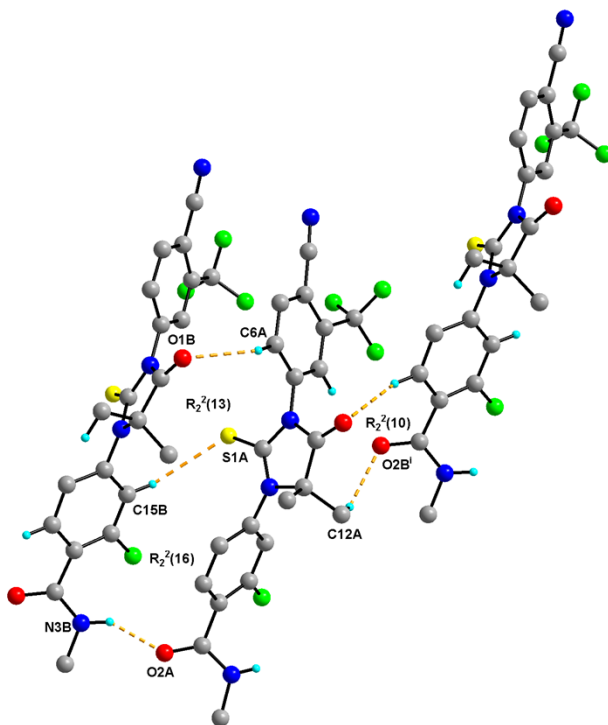
Figure S5. Part of the crystal packing of Enz-Dox 2:0.5, showing dimers between Enz molecules, which form one-dimensional chain. H atoms that are not involved in hydrogen bonding have been omitted for clarity. Hydrogen bonds are shown as dashed lines.
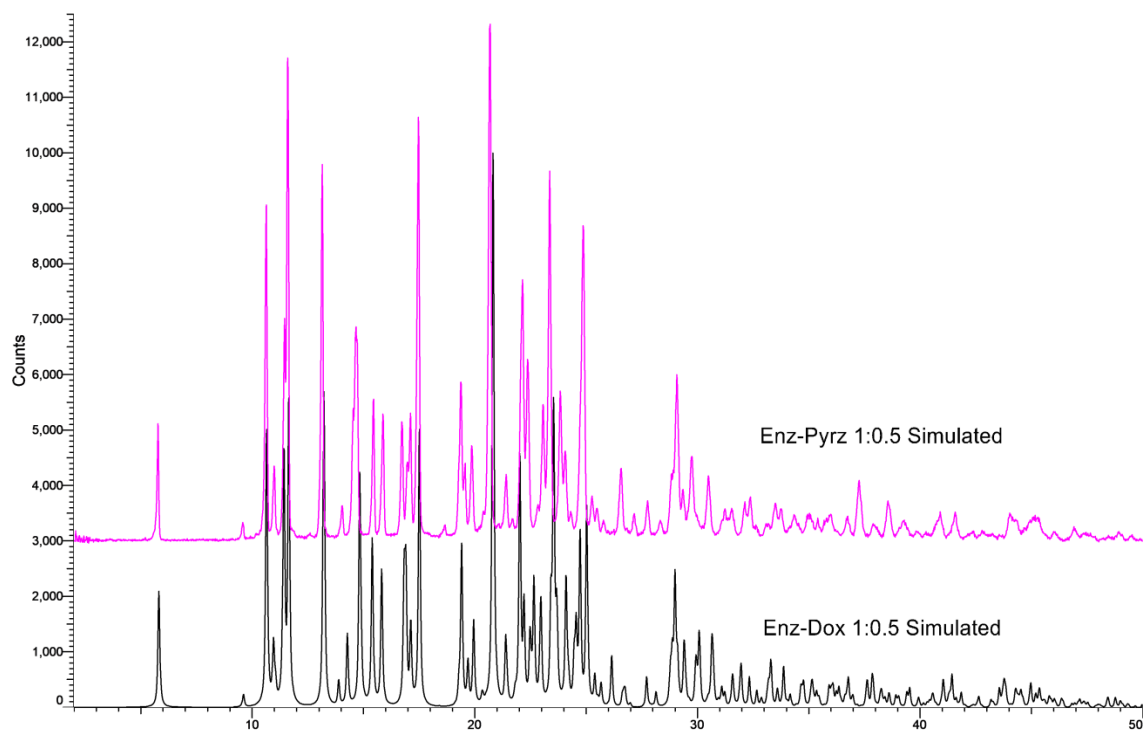

Figure S6. Overlay of simulated patterns of Enz-Dox1:0.5 and Enz-Pyrz 1:0.5.
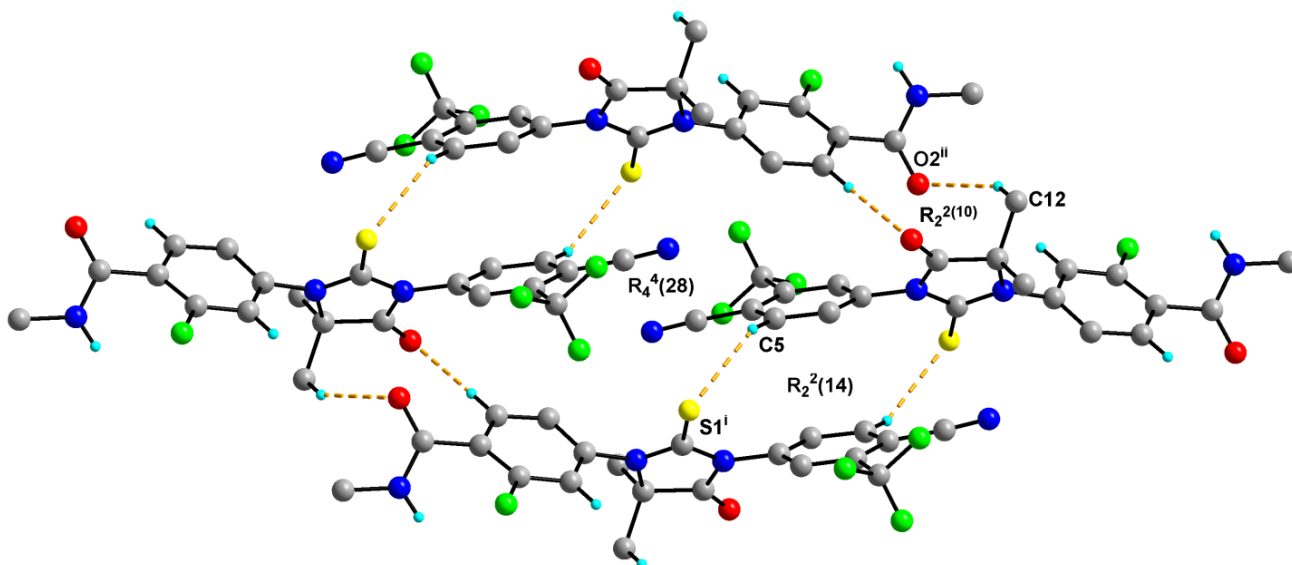
Figure S7. Enz-Pyrz 1:0.5 crystal structure showing C–H···O & C–H···S dimers which together generate a tetramer of motif ($R_4^4(28)$) and form a two-dimensional hydrogen bonded network. H atoms that are not involved in hydrogen bonding have been omitted for clarity. Hydrogen bonds are shown as dashed lines.
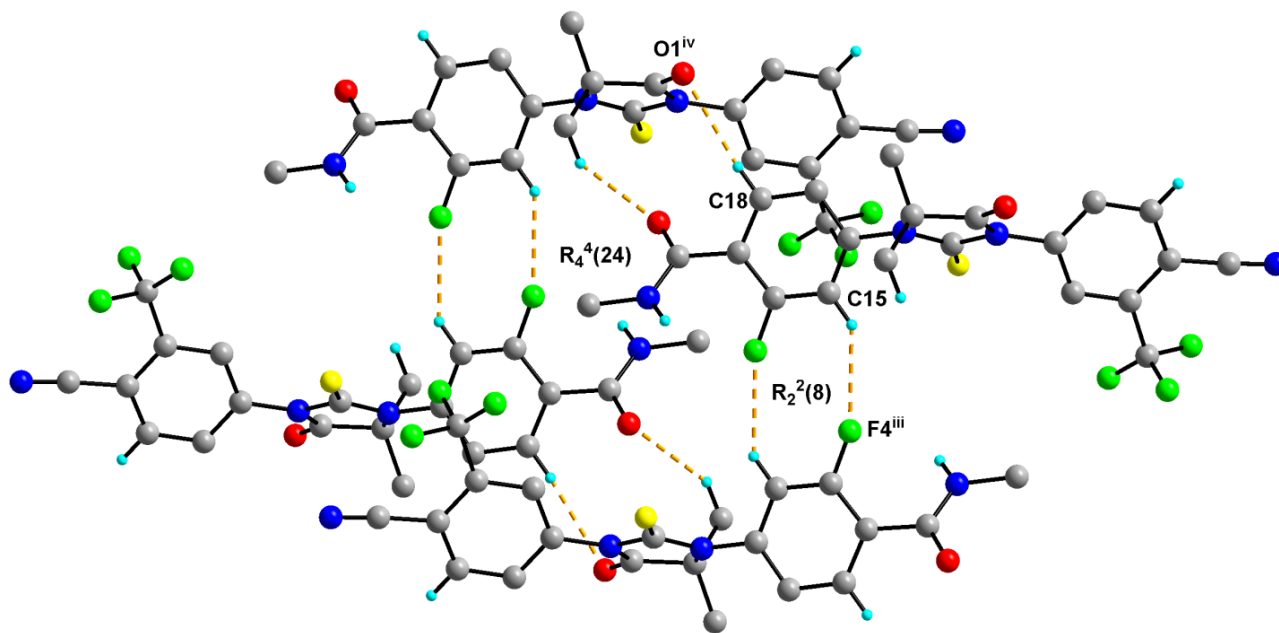
Figure S8. Crystal structure of Enz-Pyrz 1:0.5, which shows C–H···F & C–H···S dimers which in turn forms a tetramer of motif ($R_4^4(24)$) and these interactions lead to the formation of two-dimensional hydrogen-bonded network. H atoms that are not involved in hydrogen bonding have been omitted for clarity. Hydrogen bonds are shown as dashed lines.

Figure S9. Crystal packing of Enz-Pyrz 1:0.5 showing hexamer which bridges the Enz and Pyrz molecules, thereby forming three-dimensional hydrogen-bonded network. H atoms that are not involved in hydrogen bonding have been omitted for clarity. Hydrogen bonds are shown as dashed lines.
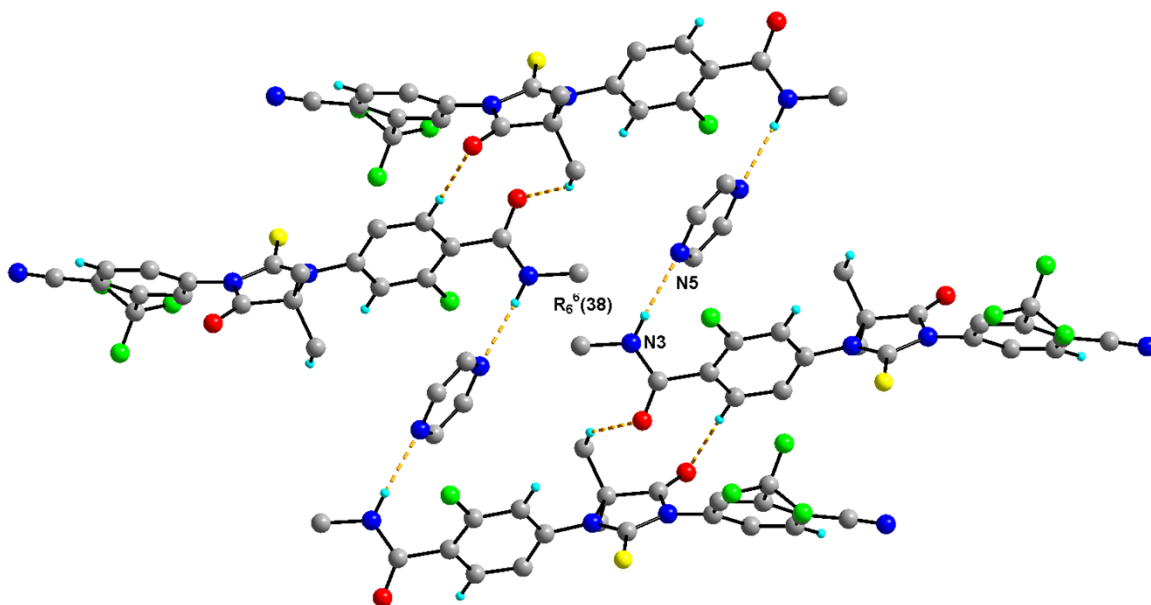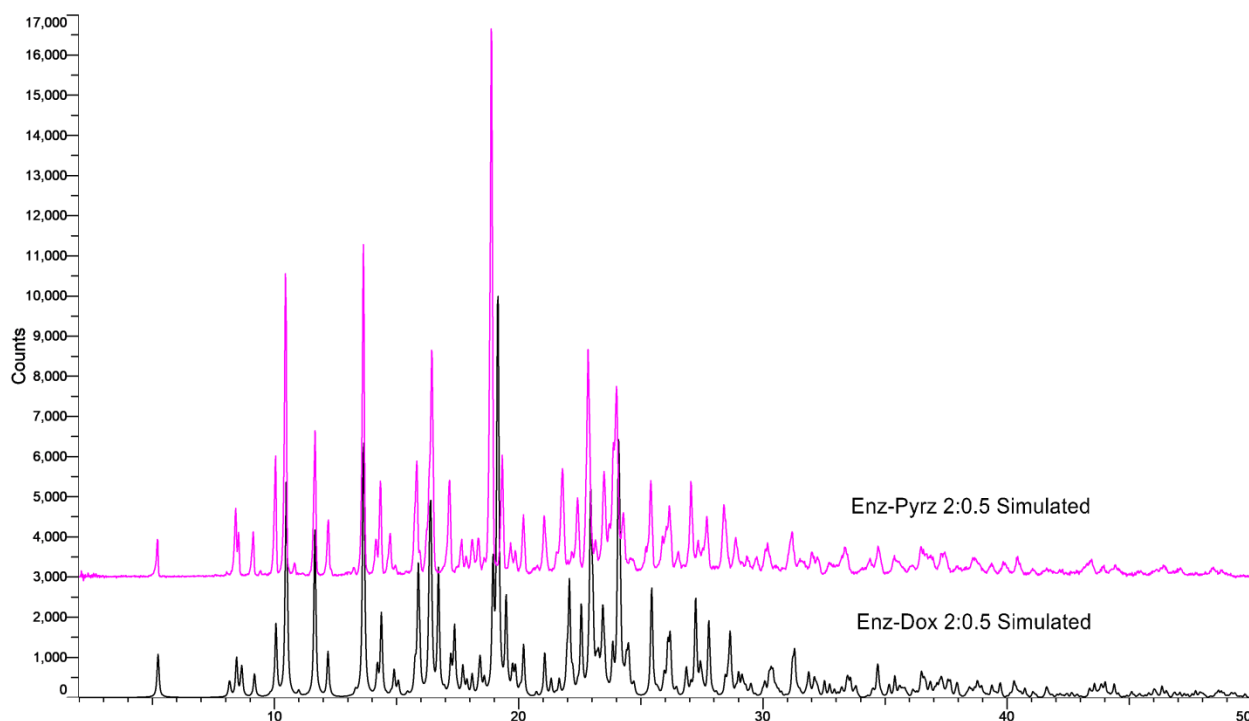

Figure S10. Overlay of simulated patterns of Enz-Dox 2:0.5 and Enz Pyrz 2:0.5.
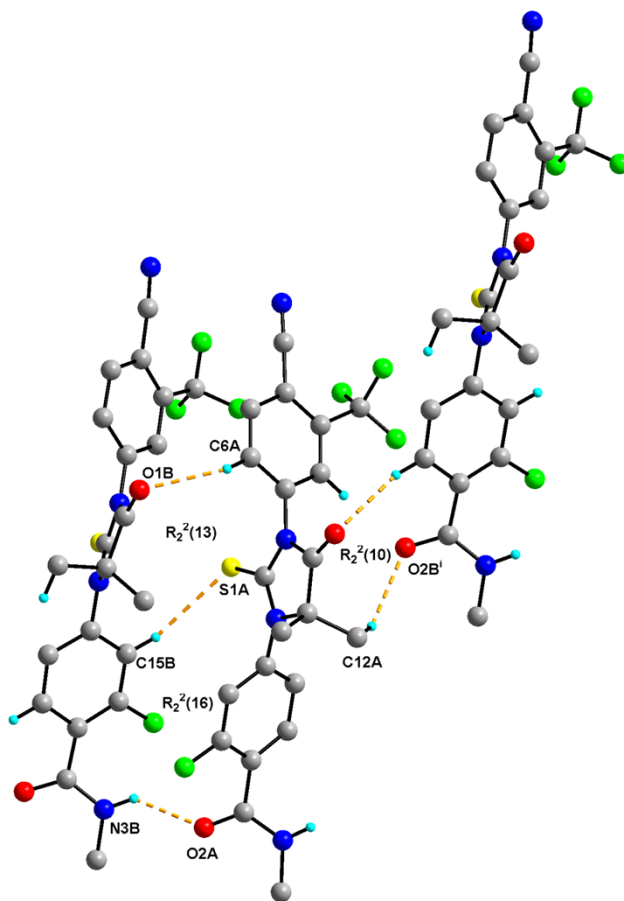
Figure S11. Part of crystal packing of Enz-Pyrz 2:0.5 depicting the dimers formed by C–H···O and C–H···S interactions which forms a 2D network. H atoms that are not involved in hydrogen bonding have been omitted for clarity. Hydrogen bonds are shown as dashed lines.
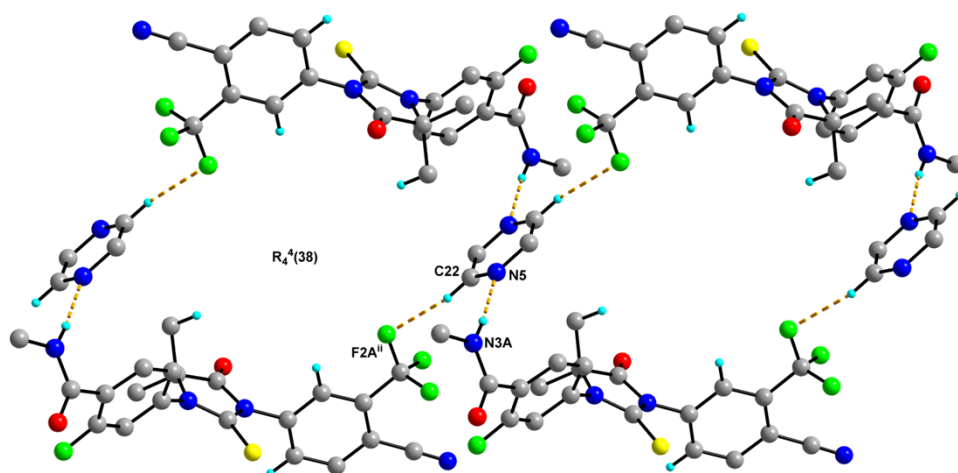
Figure S12. Enz-Pyrz 2:0.5 crystal structure showing tetramer of motif R_4^4 (38) formed by Enz A and Pyrz molecules which in turn aid in generating a 3D network. H atoms that are not involved in hydrogen bonding have been omitted for clarity. Hydrogen bonds are shown as dashed lines.

|	0	3.60	7.20	10.80	14.40	17.99	21.59	25.19	28.79	32.39	35.99

0:Enz Dox 1:0.5.cif
2:Enz Pyrz 1:0.5.cif
1:Enz Dox 2:0.5.cif
3:Enz Pyrz 2:0.5.cif

Fig S13. Packing similarity dendrogram of Enz-Dox 1:0.5, Enz-Pyrz 1:0.5, Enz-Dox 2:0.5, Enz-Pyrz 2:0.5. The PSab value (similarity) is represented on the horizontal axis. Green indicates similar and close packing arrangements, and red indicates dissimilar packing.
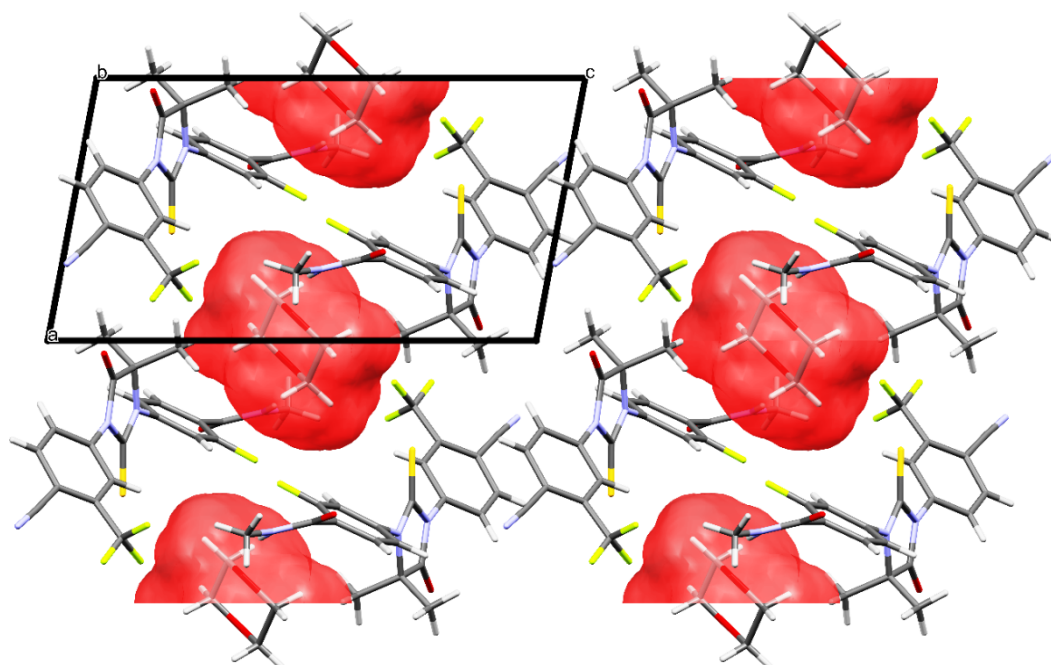
Figure S14. Packing arrangement and void map of Enz-Dox 1:0.5 along b-axis
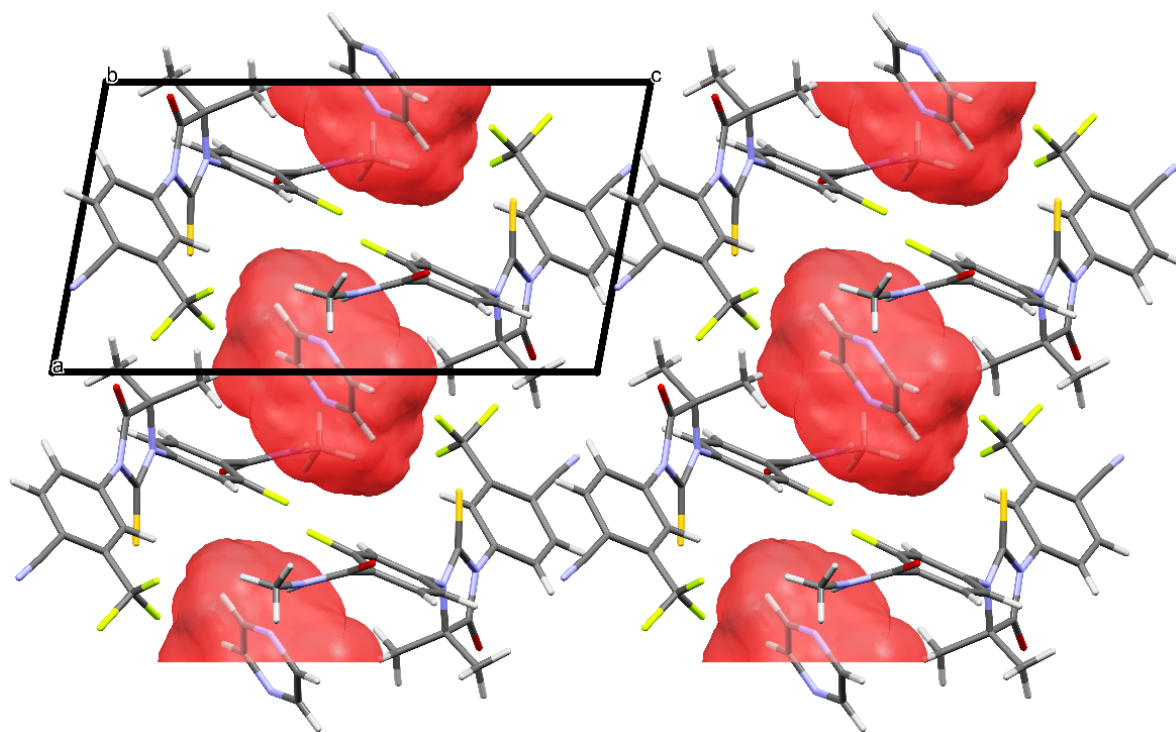
Figure S15. void map of Enz-Pyrz 1:0.5 along b-axis
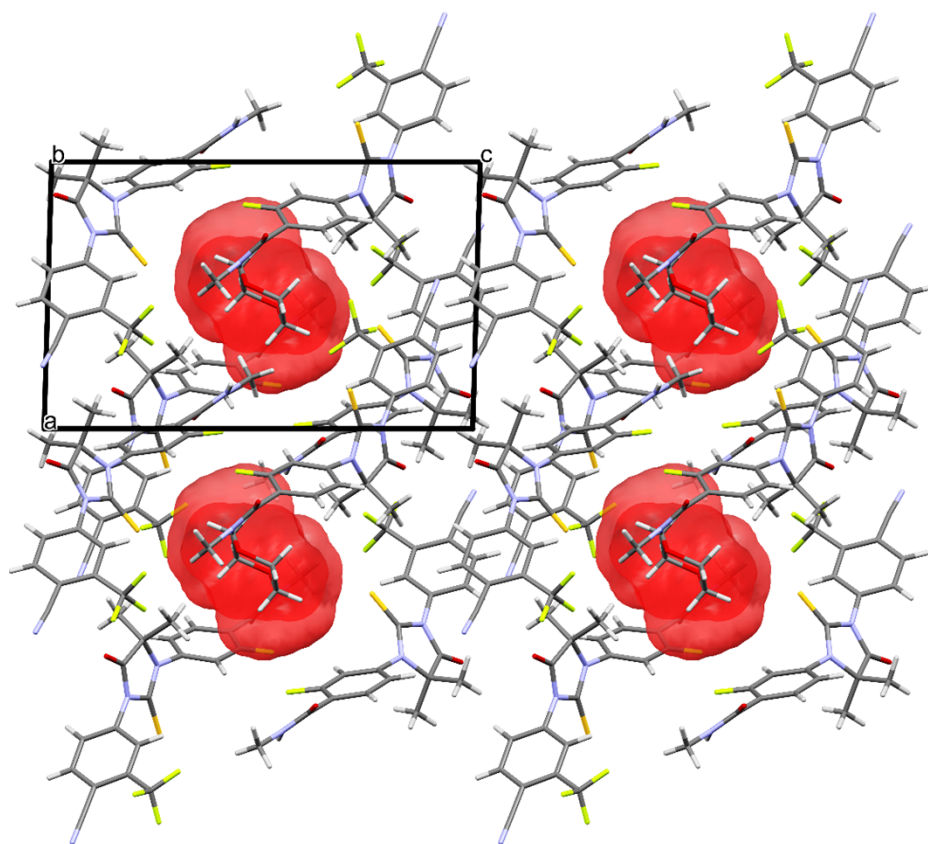
Figure S16. Packing arrangement and void maps in Enz-Dox 2:0.5 along b-axis
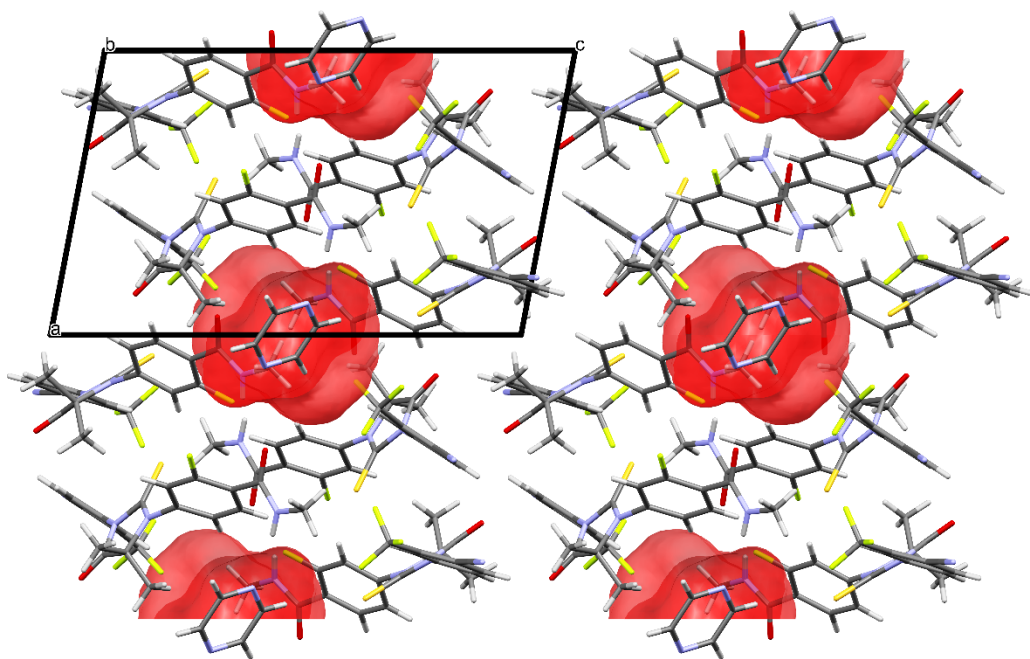
Figure S17. Pictorial representation of voids in Enz-Pyrz 2:0.5 along b-axis

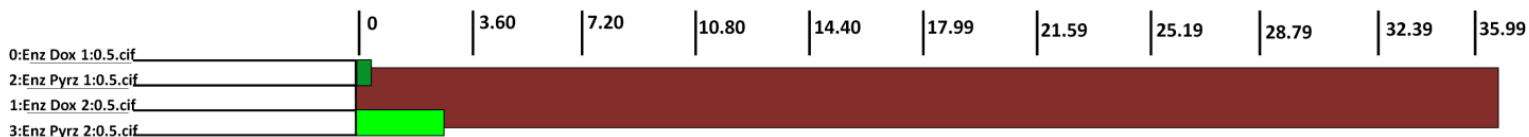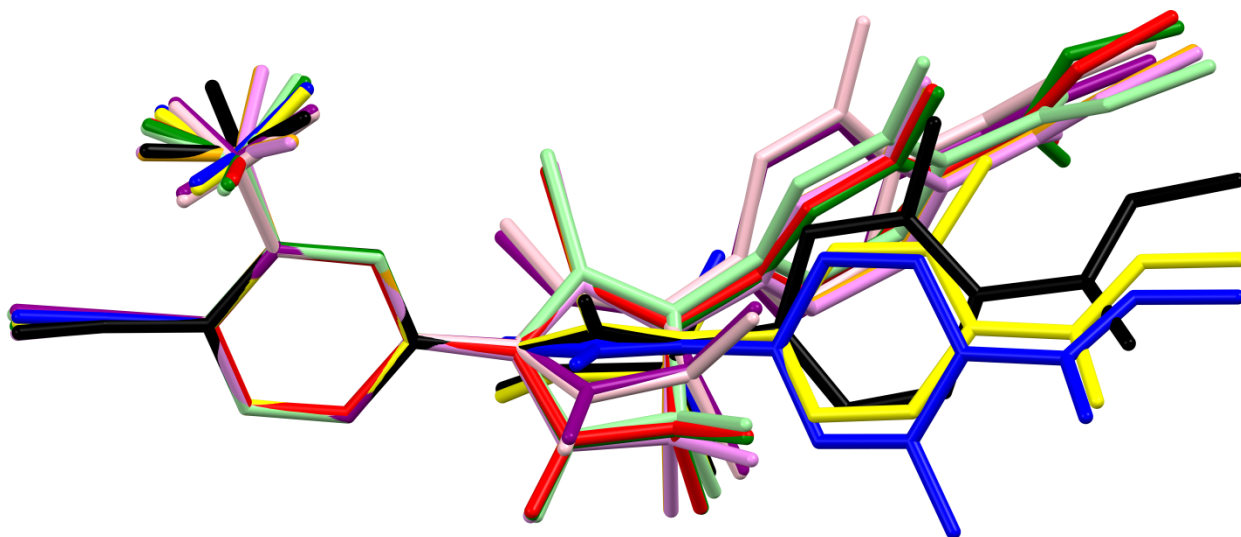Fig S18. Overlay of the molecular conformations of Enz-R2 (red), Enz·EtOH (green), [Enz+Schr] (cr) (blue), Enz-Dox 1:0.5 (black), Enz-Dox 2:0.5 Mole A (pink)/Mole B (orange), Enz-Pyrz 1:0.5 (light green), Enz-Pyrz 2:0.5 Mole A (purple)/Mole B (violet). The overlay was generated by making a least-square fit through the phenyl ring system (C1-C6) of the parent Enz (yellow). Following are the r.m.s deviations (Å): Enz-R2 (0.016), Enz·EtOH (0.0163), [Enz+Schr] (cr) (0.0113), Enz-Dox 1:0.5 (0.013), Enz-Dox 2:0.5 Mole A (0.117), Enz-Dox 2:0.5

Mole B (0.0179), Enz-Pyrz 1:0.5 (0.0217), Enz-Pyrz 2:0.5 Mole A (0.0138), Enz-Pyrz 2:0.5 Mole B (0.0169).
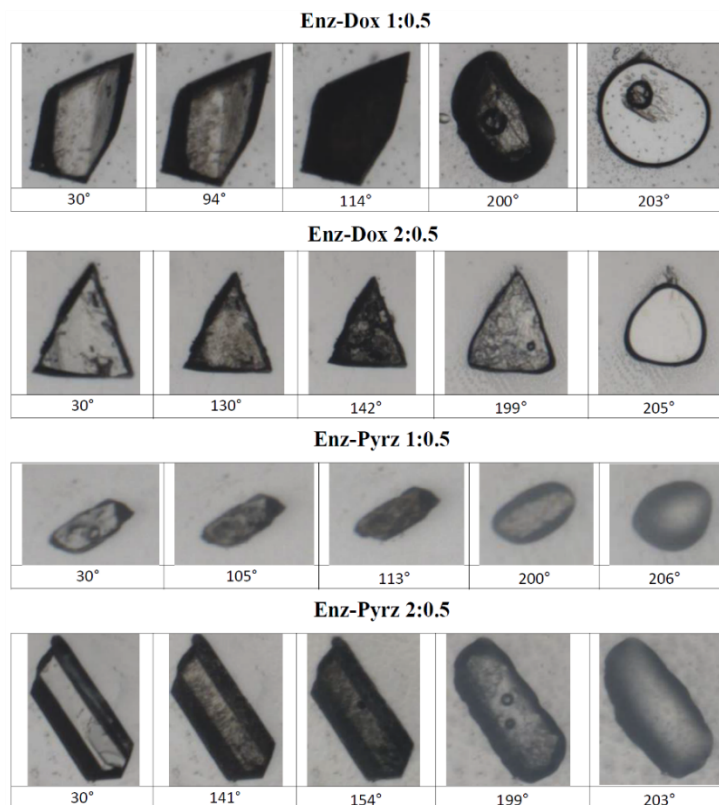
Figure S19: HSM of solvates and cocrystals.
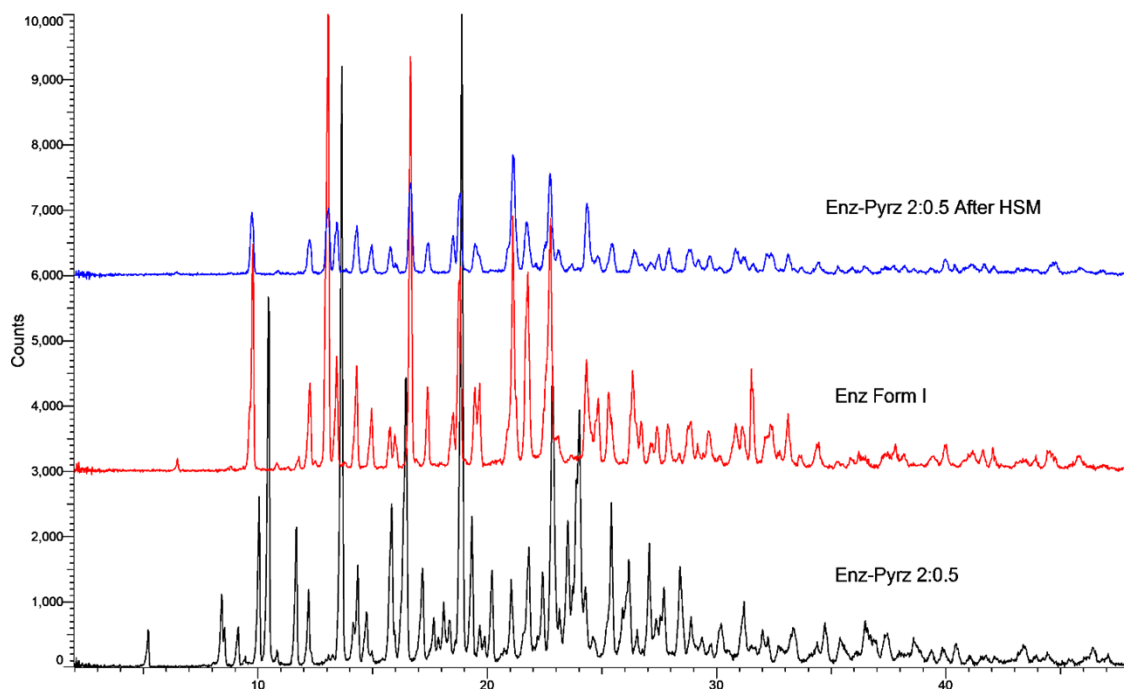
Figure. S20. PXRD overlay of Enz-Pyrz 2:0.5 cocrystal which was used for HSM experiment with the obtained form after cocrystal dissociation (Enz-Pyrz 2:0.5 Aftr HSM) and Enz Form I.
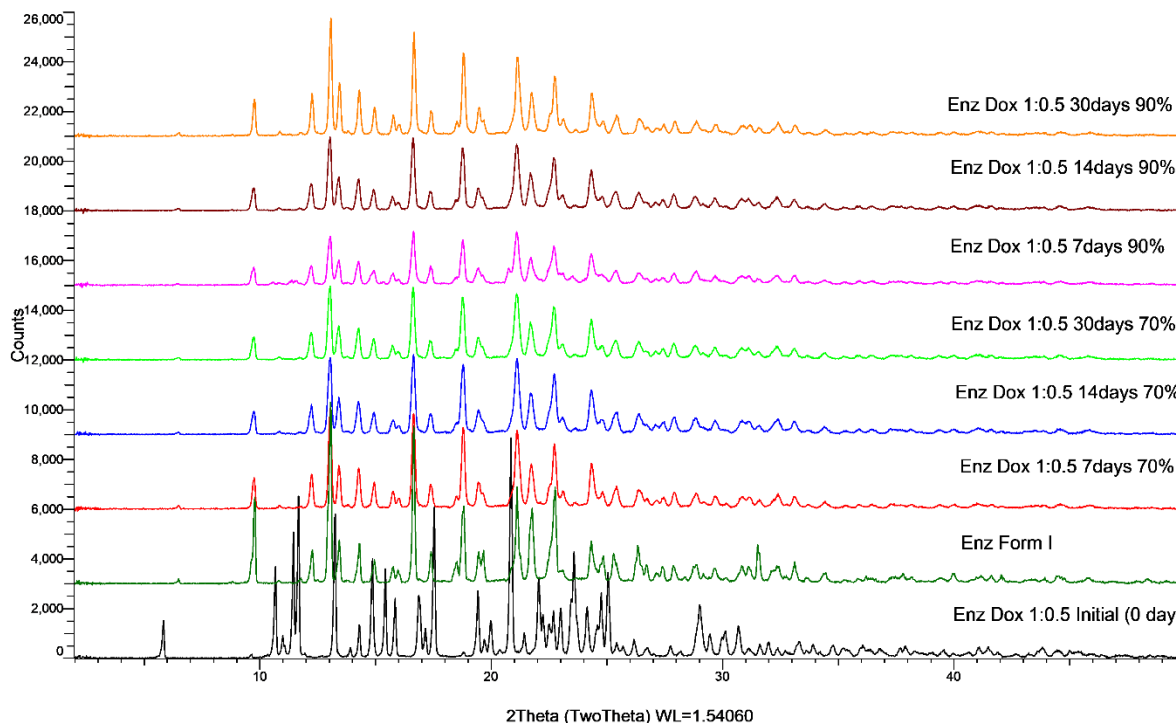
Figure S21. PXRD overlay of Enz-Dox 1:0.5 solvate samples stored at 70-75%, 90% RH conditions for 7days, 14 days and 30days.
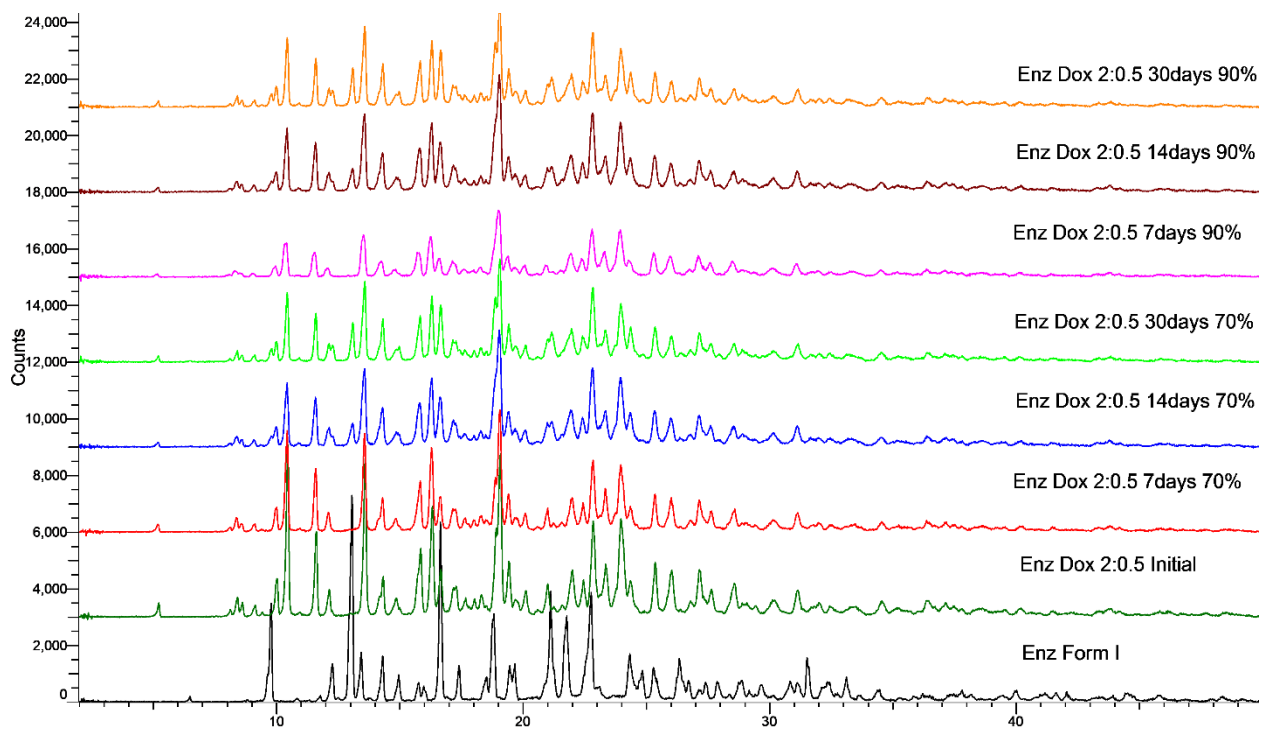
Figure S22. PXRD patterns of Enz-Dox 2:0.5 solvate samples stored at 70-75%, 90% RH conditions for 7days, 14 days and 30days.
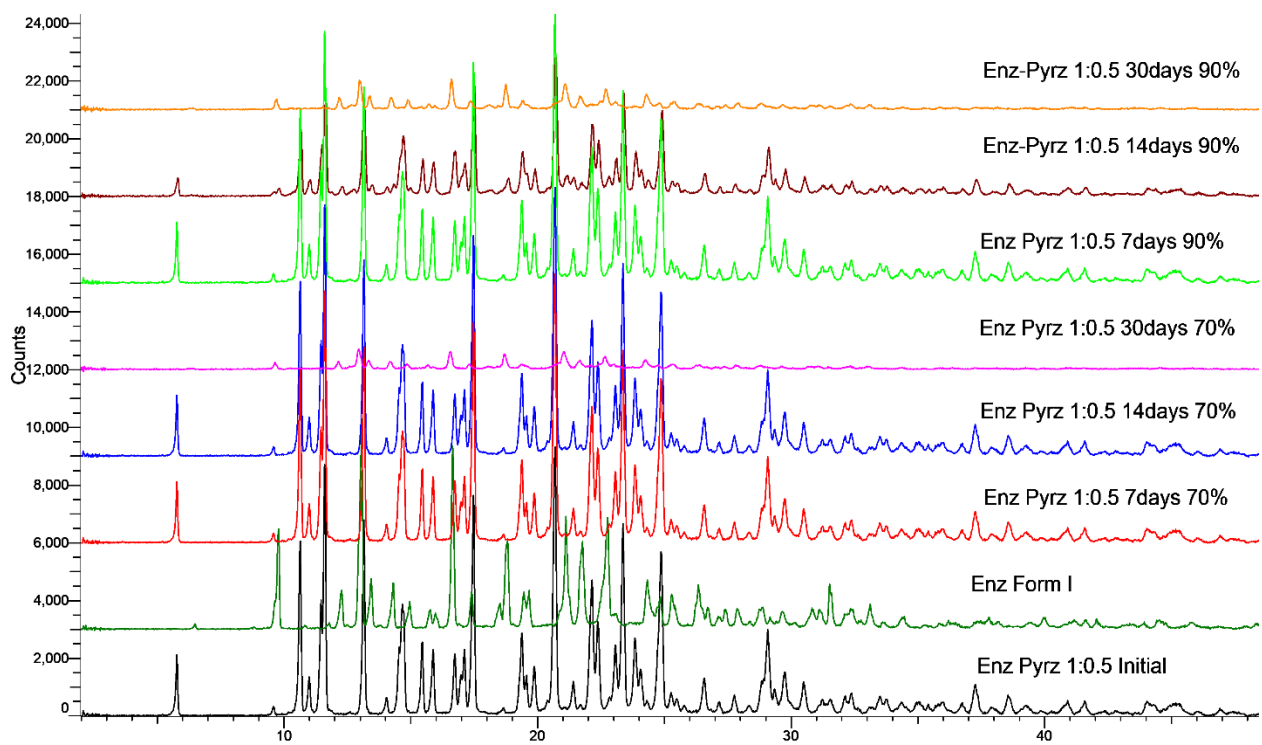
Figure S23. PXRD overlay of Enz-Pyrz 1:0.5 cocrystal samples stored at 70-75%, 90% RH conditions for 7days, 14days & 30days
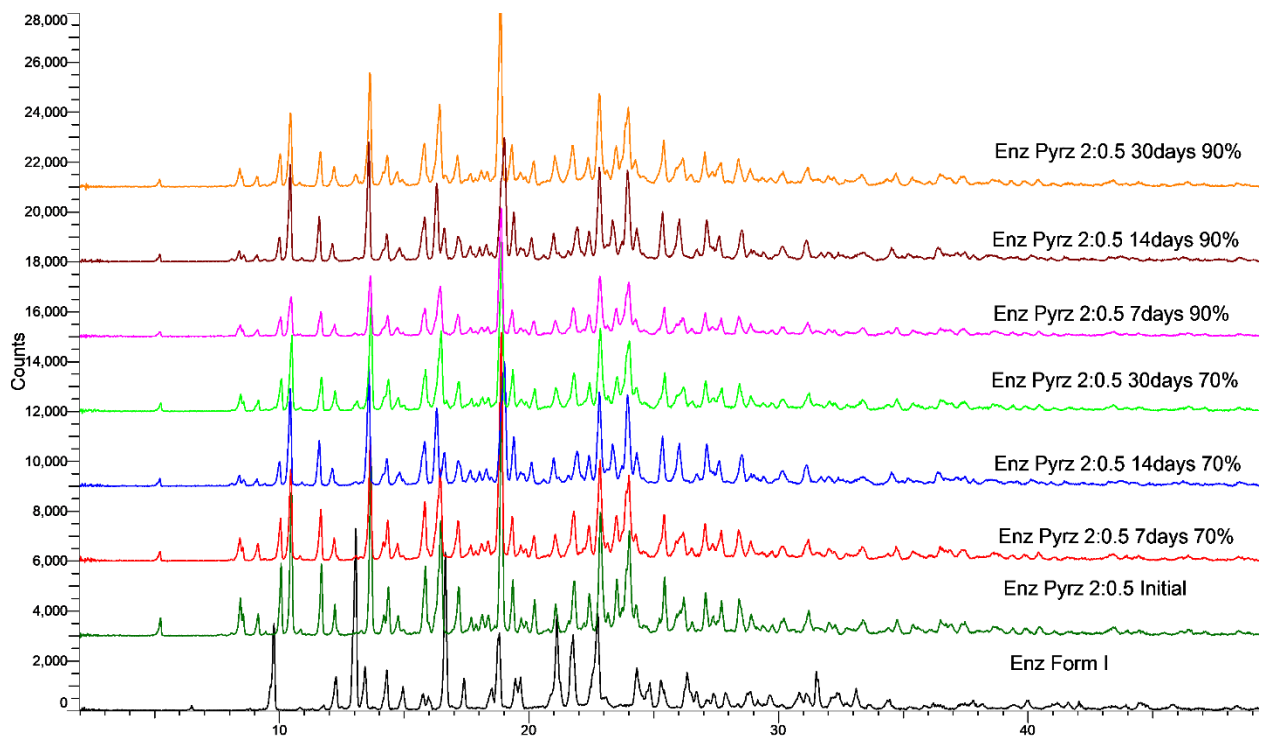
Figure S24. Pxrd patterns of Enz-Pyrz 2:0.5 cocrystal material stored at 70-75%, 90% RH conditions for 7days, 14days & 30days.
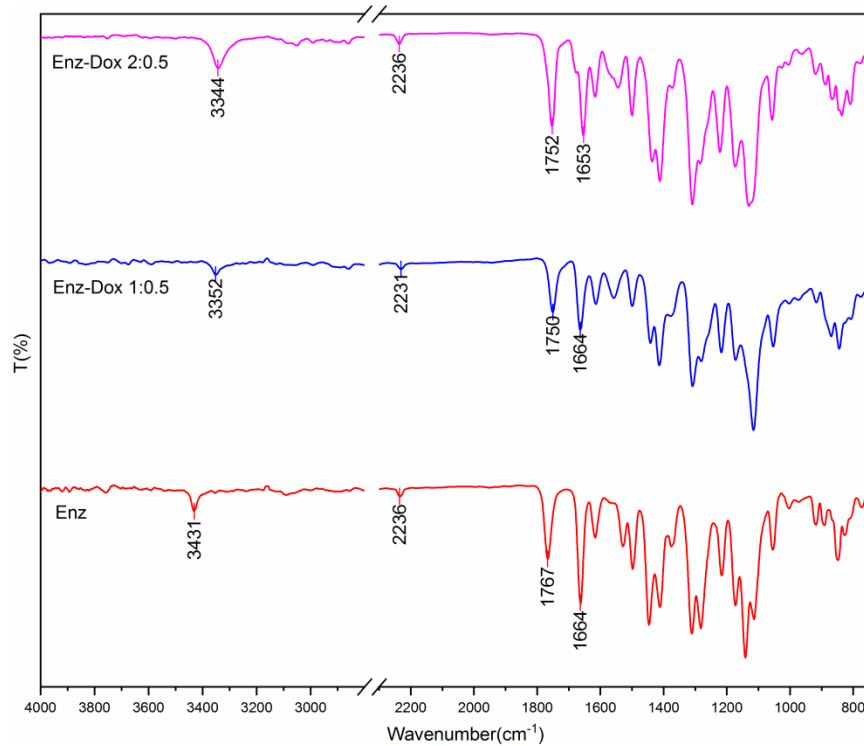
Fig.S25. Experimental FT-IR spectra of individual components (Enz, Pyrz), cocrystals
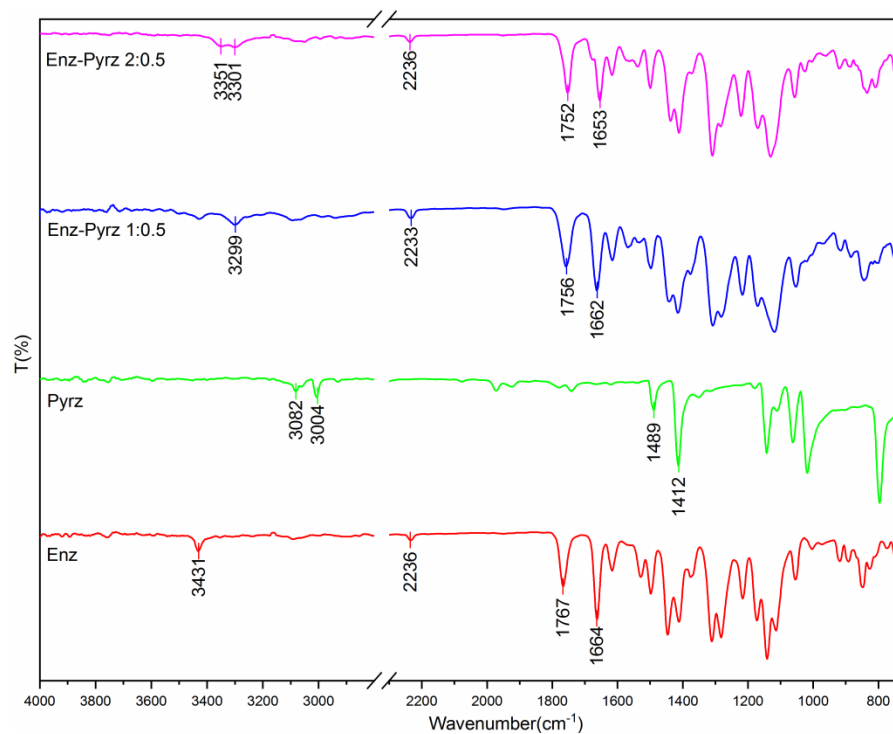
Fig. S26. Experimental FT-IR spectra of Enz, Solvates
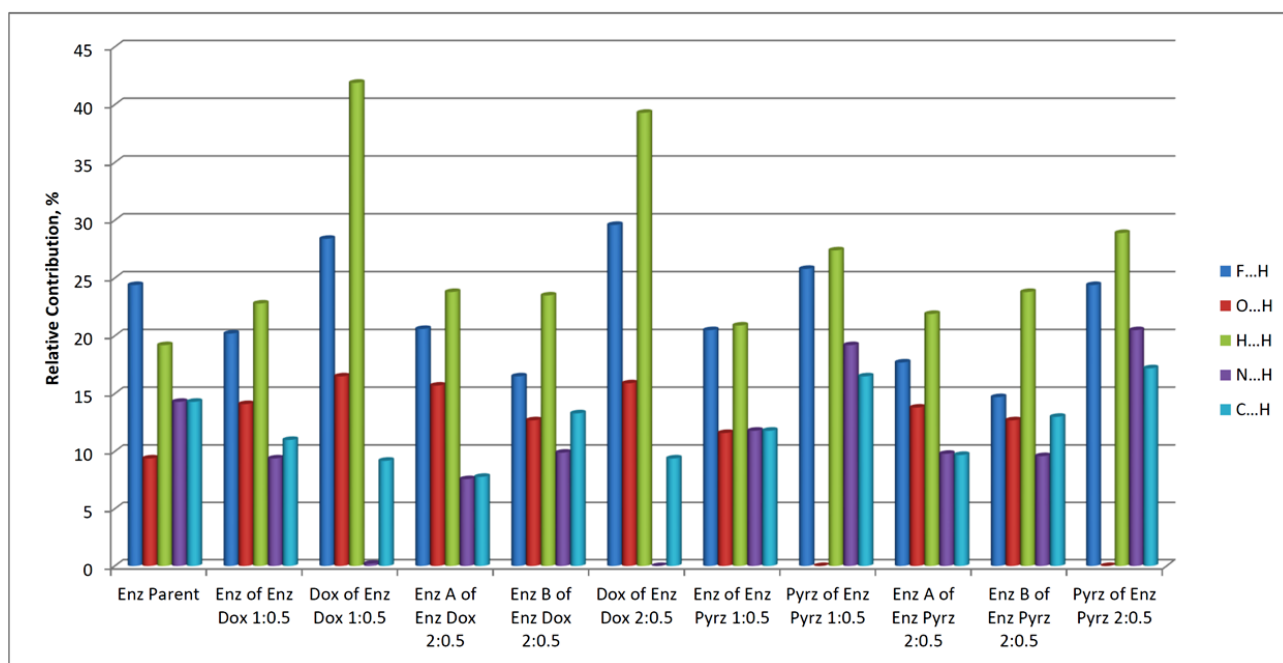
Fig S27. Hishfeld surface analysis parent of Enz and newly obtained multi-component crystals.

Table S1. Crystallographic data and structure refinement parameters of the Enz solvates and cocrystals.

|	Enz-Dox 1:0.5	Enz-Dox 2:0.5	Enz-Pyrz 1:0.5	Enz-Pyrz 2:0.5
Chemical formula	$C_{21}H_{16}F_4N_4O_2S\cdot0.5(C_4H_8O_2)$	$2(C_{21}H_{16}F_4N_4O_2S)\cdot0.5(C_4H_8O_2)$	$C_{21}H_{16}F_4N_4O_2S\cdot0.5(C_4H_4N_2)$	$2(C_{21}H_{16}F_4N_4O_2S)\cdot0.5(C_4H_4N_2)$
M_r	508.49	972.93	504.48	968.92
Crystal system, space group	Triclinic, $P\overline{1}$	Triclinic, $P\overline{1}$	Triclinic, $P\overline{1}$	Triclinic, $P\overline{1}$
Temperature (K)	100(2)	100(2)	100(2)	100(2)
a, b, c (Å)	8.3388 (8), 9.0564 (9), 15.2653 (15)	11.670 (2), 12.502 (3), 17.234 (4)	8.2956 (7), 9.1182 (8), 15.2824 (14)	11.6684 (9), 12.5374 (10), 17.0985 (13)
α, β, γ (°)	91.249 (3), 100.512 (3), 93.262 (3)	75.062 (6), 84.544 (6), 62.432 (5)	91.758 (3), 100.425 (3), 92.840 (3)	99.742 (2), 94.952 (2), 117.376 (2)
V (Å^3)	1131.04 (19)	2152.7 (7)	1134.57 (17)	2150.4 (3)
Z	2	2	2	2
Radiation type	Mo $K\alpha$	Mo $K\alpha$	Mo $K\alpha$	Mo $K\alpha$
μ (mm^{-1})	0.21	0.22	0.21	0.22
Crystal size (mm)	0.18 × 0.12 × 0.08	0.26 × 0.24 × 0.16	0.29 × 0.21 × 0.19	0.21 × 0.19 × 0.18
Data collection				
Diffractometer	Bruker D8 QUEST PHOTON-100			
Absorption correction	Multi-scan *SADABS* 2016/2: Krause, L., Herbst-Irmer, R., Sheldrick G.M. & Stalke D., J. Appl. Cryst. 48 (2015) 3-10			
T_{min}, T_{max}	0.636, 0.746	0.624, 0.746	0.691, 0.746	0.660, 0.746

No. of measured, independent and observed [$I > 2\sigma(I)$] reflections	35082, 6860, 5354	79742, 13139, 7937	26276, 6915, 4965	32888, 9833, 8038
R_{int}	0.115	0.214	0.042	0.029
$(\sin\theta/\lambda)_{max}$ (Å^{-1})	0.714	0.716	0.715	0.650
Refinement				
$R[F^2 > 2\sigma(F^2)]$, $wR(F^2)$, S	0.037, 0.098, 1.03	0.044, 0.126, 0.99	0.041, 0.101, 1.01	0.039, 0.099, 1.02
No. of reflections	6860	13139	6915	9833
No. of parameters	341	664	338	658
No. of restraints	46	170	16	48
H-atom treatment	H atoms treated by a mixture of independent and constrained refinement			
$\Delta\rho_{max}$, $\Delta\rho_{min}$ (e Å^{-3})	0.73, −0.44	0.49, −0.43	0.41, −0.33	0.86, −0.32

Table S2. Hydrogen bond geometries of Enz solvates and cocrystals				
D—H$\cdots A$	D—H	H$\cdots A$	$D\cdots A$	D—H$\cdots A$
Enz-Dox 1:0.5				
N3—H3$N\cdots$O3	0.88 (2)	2.12 (2)	2.9505 (13)	158 (2)
C5—H5$\cdots$S1^{i}	0.95	2.84	3.6909 (11)	149
C12—H12$C\cdots$O2^{ii}	0.98	2.49	3.3711 (17)	149
C18—H18$\cdots$O1^{iii}	0.95	2.53	3.4696 (14)	170
Symmetry codes: (i) −x+1, −y, −z; (ii) x, y−1, z; (iii) x, y+1, z.				
Enz-Dox 2:0.5				

N3A—H3NA···O3	0.81 (3)	2.16 (3)	2.958 (2)	169 (3)
N3B—H3NB···O2A	0.91 (3)	2.01 (3)	2.818 (3)	147 (3)
C2A—H2A···O2B[i]	0.95	2.38	3.129 (2)	136
C12A—H12C···O2B[i]	0.98	2.44	3.218 (3)	136
C13B—H13F···N4B[ii]	0.98	2.54	3.250 (3)	129
C18B—H18B···O1A[iii]	0.95	2.54	3.457 (3)	164
C6A—H6A···O1B	0.95	2.51	3.320 (2)	144
C15B—H15B···S1A	0.95	2.86	3.745 (2)	155

Symmetry codes: (i) x, $y+1$, z; (ii) $x+1$, $y−1$, z; (iii) x, $y−1$, z.

Enz-Pyrz 1:0.5

N3—H3N···N5	0.89(2)	2.18(2)	3.0342 (19)	161(2)
C5—H5···S1[i]	0.95	2.84	3.6869 (15)	148
C12—H12C···O2[ii]	0.98	2.50	3.379 (2)	149
C15—H15···F4[iii]	0.95	2.53	3.3236 (17)	141
C18—H18···O1[iv]	0.95	2.57	3.5112 (18)	170

Symmetry codes: (i) $−x+1$, $−y+2$, $−z+2$; (ii) x, $y+1$, z; (iii) $−x+1$, $−y+1$, $−z+1$; (iv) x, $y−1$, z.

Enz-Pyrz 2:0.5

N3A—H3NA···N5	0.85(2)	2.18(2)	3.034 (2)	173(2)
N3B—H3NB···O2A	0.88(2)	2.07(2)	2.825 (2)	143.3(18)
C2A—H2A···O2B[i]	0.95	2.37	3.144 (2)	138
C12A—H12C···O2B[i]	0.98	2.48	3.246 (2)	135
C13B—H13F···N4B[ii]	0.98	2.53	3.230 (2)	129
C22—H22···F2A[ii]	0.95	2.53	3.355 (3)	145

C18B—H18B···O1A[iii]	0.95	2.58	3.505 (2)	164
C6A—H6A···O1B	0.95	2.50	3.338 (2)	147
C15B—H15B···S1A	0.95	2.85	3.7347 (16)	155
Symmetry codes: (i) $x-1$, $y-1$, z; (ii) x, $y+1$, z; (iii) $x+1$, $y+1$, z.				

Table S3. Selected torsion angles for Enz-Dox (1:0.5 & 2:0.5), Enz-Dox (1:0:05 & 2:0.5), Enz parent (Enz), Enz-R2, Enz-EtOH, [Enz+Schr]$_{(cr)}$ (1:1).

Torsion angle (°)	Enz-Dox 1:0.5	Enz-Dox 2:0.5 Mole A	Enz-Dox 2:0.5 Mole B	Enz-Pyrz 1:0.5	Enz-Pyrz 2:0.5 Mole A	Enz-Pyrz 2:0.5 Mole B	Enz	Enz-R2	Enz-EtOH	[Enz+Schr]$_{(cr)}$ (1:1)
C6-C1-N1-C9 (τ_1)	48.63(13)	-86.2(2)	-49.2(2)	-48.2(19)	-90.68(19)	-48.8(2)	47.0(4)	-50.9(5)	-51.0(3)	63.5(2)
C2-C1-N1-C7 (τ_2)	45.56(14)	-78.5(2)	-51.4(3)	-45.3(2)	-82.98(18)	-52.1(2)	43.8(5)	-55.6(5)	-53.4(3)	61.7(2)
C15-C14-N2-C8 (τ_3)	107.42(11)	-97.6(2)	-110.88(19)	-104.24(16)	82.86(19)	-111.18(17)	-90.9(4)	83.0(5)	-95.2(3)	-88.82(19)
C19-C14-N2-C7 (τ_4)	117.52(11)	-109.4(2)	-120.53(19)	-114.36(16)	76.9(2)	-121.37(17)	-105.3(4)	80.4(5)	-99.7(3)	-95.28(19)
C16-C17-C20-N3 (τ_5)	-42.8(15)	52.2(3)	33.2(2)	41.4(2)	-123.59(18)	32(2)	-11.8(6)	7.0(7)	-6.1(3)	134.33(16)

Table S4. DSC observations of solvates and cocrystal forms highlight desolvation temperature (T_{desolv})/ dissociation temperature (T_{dissoc}).

Compound	T_{desolv}/ T_{dissoc}		Melting endotherm	
	T_{Onset}(°C)	T_{Peak}(°C)	T_{Onset}(°C)	T_{Peak}(°C)
Enz-Dox 1:0.5	97.20	113.20	198.93	199.93
Enz-Dox 2:0.5	128.19	141.48	199.07	200.24
Enz-Pyrz 1:0.5	101.21	118.88	198.56	200.55
Enz-Pyrz 2:0.5	138.94	151.68	198.97	199.98

Table S5. Lattice energies of multicomponent crystals E_{latt} and hypothetical desolvated crystals E_{latt}^{desolv} and binding energies of the second component in the crystal E_{bind}

Qty.	Method	Enz	Enz-Dox 1:0.5	Enz-Pyrz 1:0.5	Enz-Dox 2:0.5	Enz-Pyrz 2:0.5
E_{latt}	DFT-D3	-185.7	-240.8	-232.9	-225.3	-228.5
	CE-B3LYP	-196.6	-248.4	-232.9	-240.2	-237.9
	QTAIMC	-128.5	-211.1	-191.7	-179.4	-166.0
E_{latt}^{desolv}	DFT-D3		-172.2	-169.4	-190.2	-195.0
	CE-B3LYP		-179.7	-172.8	-204.9	-208.9
	QTAIMC		-140.7	-139.6	-148.5	-145.5
E_{bind}	DFT-D3		-68.6	-63.5	-35.2	-33.5
	CE-B3LYP		-68.7	-60.1	-35.3	-29.1
	QTAIMC		-70.5	-52.1	-61.7	-41.0

Table S6. Contributions of different types of stabilizing non-covalent interactions into the lattice energy of multicomponent crystals of enzalutamide with 1,4-dioxane and pyrazine estimated using QTAIMC scheme. All units are kJ·mol^{-1} and % of lattice energy.

	Enz-Dox 1:0.5	Enz-Pyrz 1:0.5	Enz-Dox 2:0.5	Enz-Pyrz 2:0.5
E_{latt}	211.1	191.7	358.7	332.0
Enz-Enz	140.7 (66.6%)	139.6 (72.8%)	297.0 (82.8%)	291.1 (87.7%)
Enz-[Dox/Pyrz]	70.5 (33.4%)	52.1 (27.2%)	61.7 (17.2%)	41.0 (12.3%)
$\Sigma E(N\text{-}H\cdots[O/N])$	20.3 (9.6%)	16.9 (8.8%)	44.6 (12.4%)	39.0 (11.8%)
$\Sigma E(C\text{-}H\cdots X)$ including	135.9 (64.4%)	122 (63.6%)	187.4 (52.2%)	177.9 (53.6%)
$\Sigma E(C\text{-}H\cdots O)$	31.1 (14.7%)	30.0 (15.7%)	57.1 (15.9%)	59.4 (17.9%)
$\Sigma E(C\text{-}H\cdots N)$	19.4 (9.2%)	19.6 (10.2%)	39.6 (11.0%)	32.9 (9.9%)
$\Sigma E(C\text{-}H\cdots F)$	58.8 (27.9%)	45.6 (23.8%)	43.7 (12.2%)	32.2 (9.7%)
$\Sigma E(C\text{-}H\cdots S)$	13.9 (6.6%)	18.0 (9.4%)	30.5 (8.5%)	32.3 (9.7%)
$\Sigma E(C\text{-}H\cdots\pi)$	12.7 (6.0%)	8.8 (4.6%)	16.5 (4.6%)	21.2 (6.4%)
$\Sigma E(X\cdots F)$	20.2 (9.6%)	25.4 (13.2%)	56.6 (15.8%)	51.4 (15.5%)
Pi-stacking	16.0 (7.6%)	15.9 (8.3%)	35.9 (10.0%)	38.0 (11.5%)
Other	18.8 (8.9%)	11.5 (6.0%)	34.2 (9.5%)	25.6 (7.7%)